

Phase Evolution and Sintering Kinetics of Hydroxyapatite Synthesized by Solution Combustion Technique

Swadesh K Pratihar^{*}, Mayank Garg, Supreet Mehra and S. Bhattacharyya
Department of Ceramic Engineering
National Institute of Technology
Rourkela – 769 008
India

Abstract

Solution combustion technique has been used to prepare hydroxyapatite (HAp) powder from calcium nitrate, di-ammonium hydrogen phosphate and citric acid precursors. Phase evolution has been studied as a function of calcination temperatures. The crystal structure, phase purity and stoichiometry of phase have been studied by Rietveld analysis of the calcined powder. It was observed that the prepared Hap powder was phase pure and stoichiometric. The sintering behaviour and sintering kinetics of the HAp compact has been studied by dilatometer. Activation energy for sintering has been calculated from the dilatometer results. Grain boundary diffusion was found to be the dominant densification mechanism during the initial stage of sintering. The activation energy for sintering (438 kJ/mol) was found to be in excellent agreement with reported value.

Key Words: Hydroxyapatite; combustion synthesis; sintering kinetics; activation energy

* Corresponding author: E-mail: skpratihar@nitrkl.ac.in, Phone: 91 661 2462206, Fax: 91 661 2472926

1. Introduction

Hydroxyapatite (HAp) having chemical formula $\text{Ca}_{10}(\text{PO}_4)_6(\text{OH})_2$ is being extensively used for bioimplant fabrication [1,2]. On account of the similarity in the mineral constituents between HAp and natural hard tissues (teeth and bones) it has excellent biocompatibility [3]. HAp bioceramics cannot be used for heavy load-bearing

applications, especially in aqueous environments, due to its low mechanical reliability. Thus, general usages include biocompatible phase reinforcement in composites, coatings on metal implants and granular fill for direct incorporation into human tissues [1-3]. Non-medical applications of HAp include packing media for column chromatography, gas sensors, catalyst and host materials for lasers [4]. Different properties of HAp such as bioactivity, biocompatibility, solubility, sinterability, fracture toughness and adsorption can be tailored over wide ranges by control of phase composition (e.g. lattice substitution), particle size and morphology[1-3,5]. For these reasons, it is of great importance to develop inexpensive HAp synthesis methods with emphasis on the precise control of particle size, morphology and chemical composition.

A number of methods have been used for HAp powder synthesis, such as solid state reactions, co-precipitation [6], hydrothermal reaction [7], sol-gel synthesis [8,9], microemulsion synthesis [10] and mechanochemical synthesis [11,12]. Now-a-days sol-gel processes for synthesis of HAp have become an important research objective. The sol-gel method offers a molecular-level mixing of the calcium and phosphorus precursors, which is capable of improving chemical homogeneity and reducing formation temperature of resulting HAp in comparison with conventional methods.

The citric acid solution combustion (sol-gel combustion) technique is a non-alkoxide sol-gel method. This method has been effectively used for synthesis of nanocrystalline inorganic powders [13-19]. A few attractive features of this technique are its ability to synthesize materials with high purity, better homogeneity and high surface area in a single step process [20-22]. Calcium phosphate ceramics have also been prepared by a modified combustion synthesis route which differs a little from the citric

acid sol-gel combustion route. For example, Varma et al. [23] synthesized calcium phosphate ceramics by a polymeric combustion method utilizing a solution of calcium nitrate and ethyl phosphate. Cuneyt Tas [24] synthesized calcium phosphate bioceramic powders by using a synthetic body fluid solution via the self-propagating combustion synthesis technique. Recently, Han et al. [25] have synthesized nanocrystalline HAp powder by citric acid sol-gel combustion method. However, they have not reported the phase evolution of the synthesized powder in detail. Moreover, the synthesized powder was reported to decompose to tri-calcium phosphate during sintering at 1200°C. Detailed densification behavior and densification kinetics have not been discussed in detailed.

In the present investigation, phase evolution of the HAp powder synthesized by solution combustion technique has been studied in detail. Rietveld analysis of the powder sample calcined at high temperature was performed in order to find out the crystal structure, phase purity and phase stoichiometry. Sintering behavior and sintering kinetics has been studied in detail. A possible sintering mechanism has been suggested from the kinetic study.

2. Experimental

Calcium nitrate ($\text{Ca}(\text{NO}_3)_2 \cdot 4\text{H}_2\text{O}$), di-ammonium hydrogen phosphate ($(\text{NH}_4)_2\text{HPO}_4$), citric acid monohydrate ($\text{C}_6\text{H}_8\text{O}_7 \cdot \text{H}_2\text{O}$) and HNO_3 were used as the starting precursors for the synthesis of HAp powder by solution combustion technique. All the reagents used in this study were of analytical grade. A stock solution of calcium nitrate (concentration 0.5 mol/lit) was prepared using distilled water. To 100 ml of this stock solution stoichiometric amount of di-ammonium hydrogen phosphate (3.879 gm) was added so as to get Ca/P ratio 1.67. Concentrated HNO_3 was added drop wise until the

solution pH was 2.5. The pH of the mixed salt solution was kept in the acidic range to stabilize/maintain a clear solution as well as to prevent unwanted precipitation of either one or both the reactants before the gel formation and combustion actually starts. Required amount of citric acid (10.49gm/100ml of mixed solution) was added in such a way that the citrate to nitrate ratio in the mixed solution was 0.25:1. This mixed solution was heated on a hot plate while being stirred intensely at the same time. During this stirring and heating process the mixed solution undergoes dehydration reaction and transforms into a transparent viscous gel, which on further heating burnt to yield black ash. Phase pure HAp powder was produced on calcination of this black ash. Flow diagram for synthesis of HAp powder by combustion synthesis technique is presented in Fig. 1.

Differential Thermal Analysis (DTA) of the dried transparent gel was performed in order to study the combustion and decomposition behavior of the gel. The black ash was calcined in the temperature range of 450-950°C for a holding time of 9/hrs at each calcination temperature. A sufficiently long holding time (9 hrs) at the peak temperature was provided to ensure that all the decomposition and phase formation reactions are completed. Phase evolution in the calcined Hap powders was studied using X-ray diffractometer (Model PW 1830, Philips, Holand). Cu $K\alpha_1$ radiation ($\lambda = 1.54056 \text{ \AA}$) was used as the incident X-ray beam at an accelerating voltage of 30 kV and a current of 25 mA. The powder samples were mounted on a flat XRD plate and scanned in the range $20^\circ \geq 2\theta \leq 80^\circ$ at room temperature in the continuous scan mode (scan rate of $2\theta = 2^\circ \text{ min}^{-1}$). The crystal structure, phase purity and stoichiometry of HAp powder (calcined at 1200°C for 9/hrs) was studied from the XRD pattern obtained in the step scanning mode

in the same 2θ range. The step size and the time per step were 0.02° and 10s respectively. The crystal structure was determined by Rietveld refining of the XRD pattern with MAUD software [26]. Densification behaviour of the HAp compact was studied in a dilatometer (Netzsch 402C). Powder compacts were prepared by conventional uniaxial pressing using the as calcined powder. The agglomerated particle size was measured and found to be $1.2\ \mu\text{m}$. For constant rate sintering study the samples were heated in air atmosphere at a heating rate of $3^\circ\text{C}\ \text{min}^{-1}$. For isothermal sintering study the samples were rapidly heated (heating rate $20^\circ\text{C}\ \text{min}^{-1}$) to the isothermal sintering temperature (range $950\text{-}1200^\circ\text{C}$) followed by an isothermal holding time of 2/hrs.

3. Results and Discussion

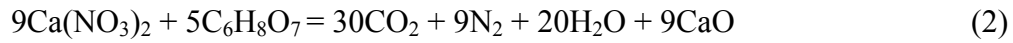
The process flow diagram for synthesis of HAp powder by solution combustion technique is presented in Fig.1. The different precursors are mixed in the sequence described in the flow diagram and a clear mixed solution is formed. During the heating of the mixed solution on hot plate it undergoes dehydration reaction followed by gelation. Among the precursors used, citric acid is a strong complex forming agent and it can form stable complex compound with many metal ions especially under acidic condition. The complex compound formation reaction may be written as follows:



This reaction prevents the precipitation of Ca^{+2} ions from solution which helps in obtaining transparent gel. Calcium citrate ($\text{C}_6\text{H}_6\text{O}_7\text{Ca}$) is very stable compound and do not contain the active groups for condensation polymerization. The cross-linking reaction of calcium citrate with the linkage of hydrogen appears to be responsible for the gelation. The viscosity of the solution increases on evaporation of the solvent from the mixed

solution as a consequence of the gelation. On heating, the solvent evaporate resulting in an increase in the viscosity of the mixed solution finally leading to gel formation.

While the citric acid used in this case acts as a fuel and is a strong reducing agent, the nitrate is a strong oxidant. Citric acid and nitrate will generate oxidation-reduction reaction leading to combustion. This combustion process leads to the formation of black ash. The black ash contains amorphous CaO, di-ammonium hydrogen phosphate and unburnt carbonaceous products from citric acid. The oxidation-reduction reaction may be written as follows:



The heat of the reaction as calculated from the heat of formation of $\text{Ca}(\text{NO}_3)_2$, $\text{C}_6\text{H}_8\text{O}_7$, CO_2 , N_2 , H_2O and CaO nearly equal to 12.5×10^3 kJ/mol. This huge amount of heat helps in the reaction of amorphous CaO with ammonium di-ammonium hydrogen phosphate to form hydroxyapatite. The possible reaction can be written as follows:



Although the above reactions indicate several stages for the formation of HAp powder by this process, the actual situation is very complex in nature and may takes place simultaneously. The black ash remains amorphous upto 450°C and crystallizes phase pure HAp powder at 550°C .

The DTA plot of the transparent gel is presented in Fig.2. The small endothermic peak at 78°C is attributed due to dehydration of water present in the gel. The sharp exothermic peak at 142°C is attributed to the oxidation reduction reaction as stated above.

Phase evolution in black ash on calcination is presented in Fig.3 as a function of calcination temperature. It can be seen from the figure that the black ash remains

amorphous below 450°C (although its colour changes from black to white on calcination at this temperature). The black colour results from the incomplete burning of the gel during combustion. This suggests that the powder formed by reaction (3) is amorphous in nature. Upon further heating to 550°C and beyond the sample crystallizes as hydroxyapatite. Each pattern shows hydroxyapatite as the only phase. The phase formed is pure and matches well with the standard pattern of hydroxyapatite (JCPDS card no. 74-0566). No other phase could be detected in the XRD pattern. The sample calcined at lower temperature exhibited broad peaks which increase in sharpness when the calcination temperature increases due to crystal growth. The crystallite size of the powder has been calculated as a function of calcination temperature by means of the X-ray line broadening method [27] using the Scherrer equation:

$$D = (0.9\lambda / \beta \sin\theta) \quad (4)$$

Where D is the crystallite size, λ is the wavelength of the radiation (1.54056 Å^o for Cu-K α_1 radiation), β is the corrected peak width at half-maximum intensity, and θ is the peak position. Silicon standard was used to measure the instrumental broadening in order to correct the value of β . The strongest peak of HAp ($2\theta = 31.766^\circ$ and $d = 2.8146$ Å^o) was used to calculate the crystallite size. The variation in crystallite size with calcination temperature is presented in Fig.4. At 550°C, the crystallize size of HAp powder is 12 nm and it increases to 58 nm at 950°C. The increase in crystallite size is found to follow two distinct steps. One in the low temperature range (550-750°C), where the increase in crystallite size is slow and the other in the high temperature ranges 750-950°C, where it increases rapidly. The slow growth rate in the low temperature range may be ascribed to the nucleation of large number of crystals. In this stage nucleation is the

predominant mechanism. In the second stage growth of the nucleated crystals takes place at a rapid rate. The diffusion controlled coarsening of the powder on heating results in an increase in the crystallite size.

The crystal structure, phase purity and stoichiometry of the HAp powder was studied by carrying out Rietveld analysis of the XRD pattern of the powder sample calcined at 1200°C and the fitted pattern is shown in Fig.5. The refinement was carried out on the basis of initial atomic parameters (S.G. P63/m) obtained from neutron diffraction data [28]. Occupancy, atom position, unit cell, peak profile, 2θ zero, preferred orientation, and background parameters were allowed to vary. The different refined parameters are given in Table - 1. The parameters determined with the Rietveld analysis of the XRD pattern are in good agreement with Wilson et al. [29], and confirm the stoichiometry and phase purity of the powder at 1200°C.

Constant rate sintering behavior of the HAp compact is plotted in Fig.6. It can be seen from the figure that the sample undergoes expansion in the temperature range 30-850°C followed by shrinkage in the temperature range 850-1200°C. The thermal expansion calculated in the lower temperature range (30-850°C) is $13.48 \times 10^{-6}/K$. The value is in good agreement to the reported thermal expansion coefficients of calcium phosphate apatite [30-32]. Therefore, two distinct stages are identified in the sintering behavior of the hydroxyapatite. The first stage is associated with particle coalescence up to 850°C and the second stage is associated with the sintering above the temperature range in which the densification mechanism becomes active [32]. The calculated densification rate $[d(dL/L)dT]$ as a function of temperature is also plotted in Fig.6 (dotted line). This curve shows a sharp peak at 1045°C with the onset of the peak at 850°C. The

densification rate is negligible in the temperature range 30-850°C and then it increases rapidly. The densification rate reaches the maximum value at 1045°C. The negligible densification rate in the temperature range 30-850°C indicate lack of appreciable densification in the samples in this temperature range. At higher temperatures (> 1045°C) the sample reaches the final stage of sintering and as a result the densification rate decreases. Thus the initial stage of sintering for the HAp compact takes place in the temperature ranges 850-1045°C. Similar type of densification behaviour was earlier reported by Juang et al. [33].

It may be noted that in constant heating rate, the observed shrinkage of the samples with temperature (Fig. 6) is equivalent to the shrinkage as a function of sintering time. Thus Fig. 6 can be used to study the sintering kinetics of the HAp compacts. For initial stage of sintering the activation energy of densification can be calculated from linear shrinkage vs temperature curve following the expression [34, 35].

$$[(dL/L)/T] = \text{Const.} \times \exp(-nE_a/RT) \quad (5)$$

or

$$[d(dL/L)/dT] T = \text{const.} \times \exp(-nE_a/RT) \quad (6)$$

Where, dL/L is the relative shrinkage at temperature T , E_a is the activation energy and n is a constant describing the sintering mechanism ($n = 1, 0.5$ and 0.33 for viscous, volume diffusion or grain-boundary diffusion respectively). Equation (5) can be rewritten as follows:

$$\text{Ln}[(dL/L)/T] = \text{Ln}(\text{Const.}) - nE_a/RT \quad (7)$$

Hence, the plot of $\text{Ln}[(dL/L)/T]$ vs $1000/T$ will be a straight line with slope equals to nE_a . Here, the temperature range will be limited only to the initial stage of sintering (in

the present investigation it is 850 – 1045°C). The calculated values were plotted in Fig.7. The open circles are the experimental values and the solid line is the fitted line. The slope of the line calculated from the fitting equation was found to be -31.473.

Isothermal sintering behaviour of HAp compact in the temperature ranges (950-1150°C is presented in Fig. 8. It can be seen from the figure that percent theoretical density of the HAp compact has a strong temperature dependence. The HAp compact attains 98% theoretical density at 1150°C/2hrs. Sintering activation energy for the HAp compact has been calculated from the isothermal dilatometer curves using Ivensen's Model [36], which is valid for all the three sintering stages (viz. initial, intermediate and final stage).

$$V_s/V_o = (1+Kt)^{-n} \quad (8)$$

Where, V_s is the volume of the sample at time t ; V_o is the volume of the sample when it reaches the isothermal temperature; time t is the holding time during isothermal segment only; K is a temperature dependent constant; n is a constant. Equation (8) also describes the change in the relative volume (V_r) ($V_r = V_s/V_o$), where, V_r is the relative volume at time t . The relative volume V_r at time t can be calculated for each sample by using the shrinkage data from the dilatometer using the following equation:

$$V_r = (1-x)^3 \quad (9)$$

Where, x is the shrinkage at time t . Equation (8) can then be rewritten as:

$$V_r = A(1+Kt)^{-n} \quad (10)$$

Where, A and n are constants; K is a temperature dependent constant. The temperature dependent constant K follows an Arrhenius relationship with temperature (T) as follows:

$$K = K_0 \exp (-E/RT) \quad (11)$$

Where, E is the activation energy for densification; K_0 is a constant and R is gas constant.

Fig. 9 shows the plot of V_r (calculated from dilatometer shrinkage data) as a function of sintering time at different isothermal temperature. The points are the experimental data and the solid lines are nonlinear curves obtained using equation (10). The constant K has been calculated from the fitted curve. $\ln(K)$ has been plotted against $1000/T$ in Fig.10. The open circles in the figure represents the experimental data, the solid line represent the fitted line. The slope of the line has been calculated from the linear fitting of the experimental data. The activation energy calculated from the slope of the line is 438 kJ/mol. The activation energy is in good agreement with the value 400-500 kJ/mol reported in the earlier studies [33,37] for stoichiometric hydroxyapatite. The densification mechanism during initial stage of sintering has been found by equating the slope of Fig. 10 with the slope of the line of Fig. 7. The observed value of $n = 0.33$ exactly matches with the reported value. Thus it can be concluded that the densification of HAp compact is controlled by grain boundary diffusion during initial stage of sintering.

4. Conclusions

Phase pure, stoichiometric hydroxyapatite can be prepared using solution combustion technique. The synthesized powder remains amorphous after combustion. Crystallization of pure hydroxyapatite phase takes place from the amorphous material on calcination at high temperature. The synthesized material remains phase pure and stoichiometric up to 1200°C. Grain boundary diffusion was found to be the predominant

mechanism during the initial stage of sintering of the hydroxyapatite compact. The densification activation energy was found to be 438 kJ/mol.

References

- [1]. L.L. Hench, *J. Am. Ceram. Soc.* **74** (1991) 1487.
- [2]. H. Aoki, in “Science and medical applications of hydroxyapatite” (Japanese Association of Apatite Science, Tokyo, Japan) 1991.
- [3]. W. Suchanek, M. Yoshimura, *J. Mater. Res.* **13** (1998) 94.
- [4]. K. Yamashita, T. Kanazawa, in “Inorganic phosphate materials” T. Kanazawa (Ed.) (Kodansha & Elsevier, Tokyo and Amsterdam, 1989) p. 15.
- [5]. R.Z. LeGeros, in “Calcium phosphates in oral biology and medicine” (Karger, Basel, Switzerland) 1991.
- [6]. L. Bernard, M. Freche, J.L. Lacout, B. Biscans, *Powder Technol.*, **103** (1999) 19.
- [7]. H.S. Liu, T.S. Chin, L.S. Lai, S.Y. Chiu, K.H. Chung, C.S. Chang, M.T. Liu, *Ceram. Int.*, **23** (1997) 19.
- [8]. D.-M. Liu, T. Troczynski, W.J.T. Seng, *Biomaterials*, **22** (2001) 1721.
- [9]. D.-M. Liu, Q. Yang, T. Troczynski, W.J. Tseng, *Biomaterials*, **23** (2002) 1679.
- [10]. G.K. Lim, J. Wang, S.C. Ng, C.H. Chew, L.M. Gan, *Biomaterials*, **18** (1997) 1433.
- [11]. K.C.B. Yeong, J. Wang, S.C. Ng, *Biomaterials*, **22** (2001) 2705.
- [12]. W.L. Suchanek, P. Shuk, K. Byrappa, R.E. Riman, K.S. TenHuisen, V.F. Janas, *Biomaterials*, **23** (2002) 699.
- [13]. D.A. Fumo, M.R. Morelli, A.M. Segadaes, *Mater. Res. Bull.*, **31** (1996)1243.
- [14]. T. Ye, Z. Guiwen, *Mater. Res. Bull.*, **32** (1997) 501.
- [15]. D.A. Fumo, J.R. Jurado, A.M. Segadaes, J.R. Frade, *Mater. Res. Bull.*, **32** (1997) 1459.
- [16]. R.E. Juo´rez, D.G. Lamas, G.E. Lascalea, N.E. Walsoe de Reza, *J. Eur. Ceram. Soc.*, **20** (2000) 133.
- [17]. H. Taguchi, S. Yamada, M. Nagao, Y. Ichikawa, K. Tabata, *Mater. Res. Bull.*, **37** (2002) 69.
- [18]. R.K. Selvan, C.O. Augustin, L.J. Berchmans, R. Saraswathi, *Mater. Res. Bull.*, **38** (2003) 41.
- [19]. J. Huang, H. Zhuang, W.L. Li, *Mater. Res. Bull.*, **38** (2003) 149.
- [20]. M. Muthuraman, K.C. Patil, *Mater. Res. Bull.*, **33** (1998) 655.
- [21]. K. Adhikary, M. Takahashi, Sh. Kikkawa, *Mater. Res. Bull.*, **33** (1998)1845.
- [22]. R. Sukumar, W. Liwu, S. Wolfgang, A. Fritz, *Mater. Lett.*, **39** (1999)138.
- [23]. H.K. Varma, S.N. Kalkura, R. Sivakumar, *Ceram. Int.*, **24** (1998) 467.
- [24]. A.Cuneyt Tas, *J. Eur. Ceram. Soc.*, **20** (2000) 2389.
- [25]. Y. Han, S. Li, X. Wang, X. Chen, *Mater. Res. Bull.*, **39** (2004) 25.
- [26]. MAUD stands for Material Analysis Using Diffraction. It is based on the RITA/RISTA method by H.-R. Wenk, S. Matthies and L. Lutterotti, Berkeley, University of California, Version 1.999 (3rd December 2003).
- [27]. Klug, H. and Alexander, L.E., in “X-ray diffraction procedures for polycrystalline and amorphous materials” (John Wiley and Sons, New York, 1974) p. 618-708.

- [28]. K. Sudarsanan and R.A. Young, *Acta Crystallogr., B*, **25** (1969) 1534.
- [29]. R.M. Wilson, J.C. Elliott and S.E.P. Dowker, *Am. Mineral.*, **84** (1999) 1406.
- [30]. G.R. Fischer, P. Bardhan, and J.E. Geiger JE, *J. Mater. Sci. Lett.*, **2** (1983) 577.
- [31]. S. Nakamura, R. Otsuka, H. Oaki, M. Akao, N. Miura, and T. Yamamoto, *Thermochim. Acta*, **165** (1990) 57.
- [32]. S. Raynaud, E. Champion, D. Bernache-Assollant, *Biomaterials*, **23** (2002) 1073.
- [33]. H.Y. Juang and M.H. Hon, *Biomaterials*, **17** (1996) 2059.
- [34]. F. Tietz, F. J. Dias, D. Simwonis and D. Stover, *J. Euro. Ceram. Soc.*, **20** (2000) 1023.
- [35]. W.S. Young and I.B. Cutler, *J. Am. Ceram. Soc.*, **53** (1970) 659.
- [36]. V.A. Ivensen, in “Densification of metal powders during sintering” Consultants Bureau, New York, 1973.
- [37]. S. Bailliez, and A Nzihou, *Chem. Eng. J.*, **98** (2004) 141.

List of Figures and Tables

- Fig. 1 Flow diagram of hydroxyapatite powder synthesis by combustion synthesis technique.
- Fig.2 DTA curve of transparent gel.
- Fig.3 XRD pattern of calcined hydroxyapatite powder as a function of calcination temperature.
- Fig.4 Crystallite size of hydroxyapatite powder as function of calcination temperature.
- Fig. 5 Rietveld refined XRD pattern of hydroxyapatite powder calcined at 1200°C/9hrs.
- Fig. 6 Constant rate sintering behaviour of hydroxyapatite compact: solid line linear shrinkage vs sintering temperature, dotted line linear shrinkage rate vs sintering temperature.
- Fig. 7 $\ln[(dL/L)/T]$ vs $1000/T$ plot for the initial stage of sintering (850-1045°C). The values of dL/L for different temperature has been taken from Figure 5.
- Fig. 8 Isothermal sintering behaviour of hydroxyapatite compact at different isothermal temperature.
- Fig. 9 Relative volume (V_r) calculated from dilatometer data as a function of sintering time. (open circles are the experimental data; solid lines are the fitted curves using Ivensen's model).
- Fig. 10 $\ln K$ vs $1000/T$ plot for activation energy calculation.
- Table 1 Crystal structure and other parameters determined from Rietveld analysis. Crystal structure has been refined using hexagonal structure and space group: P63/m.

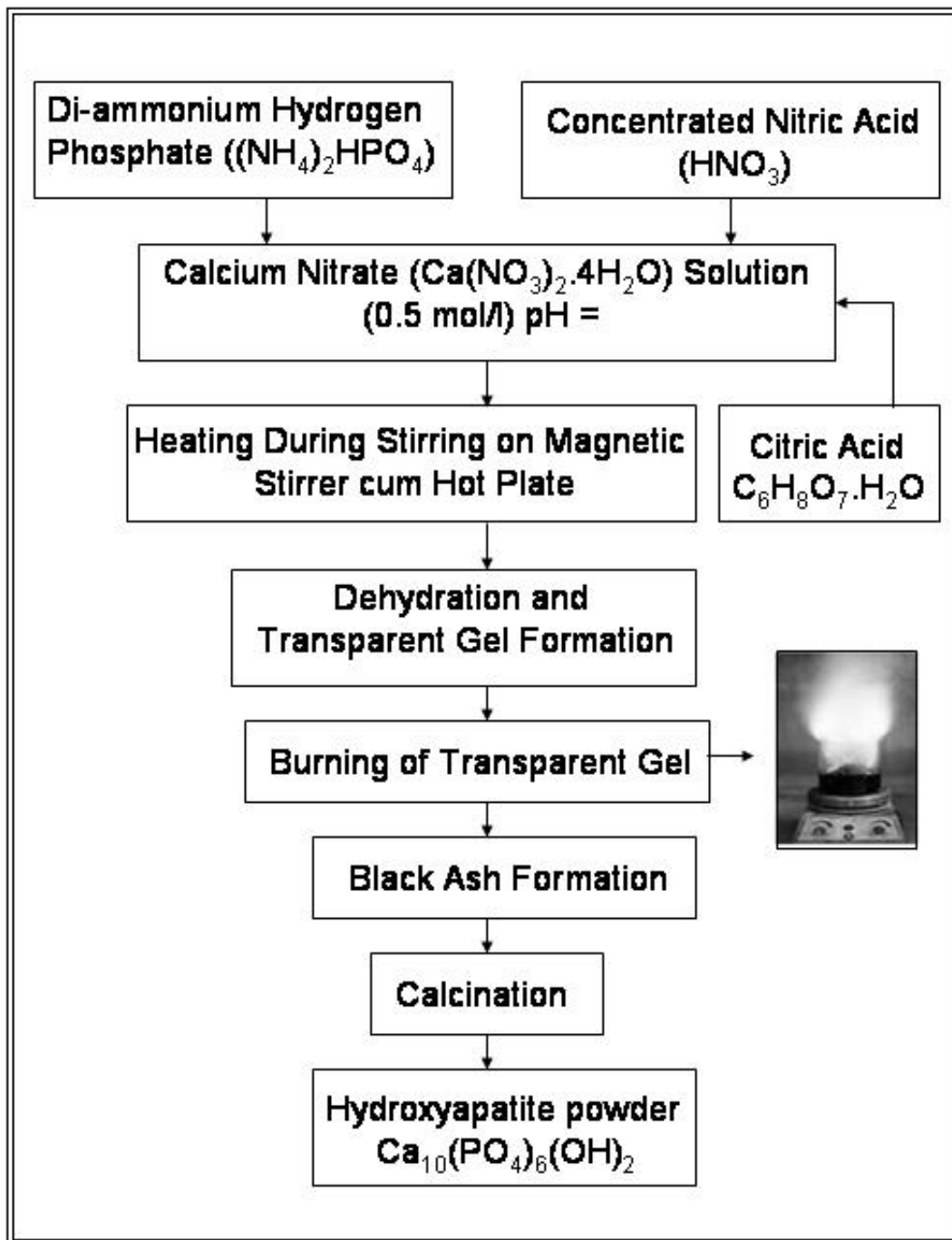


Fig. 1 S.K. Pratihari et al.

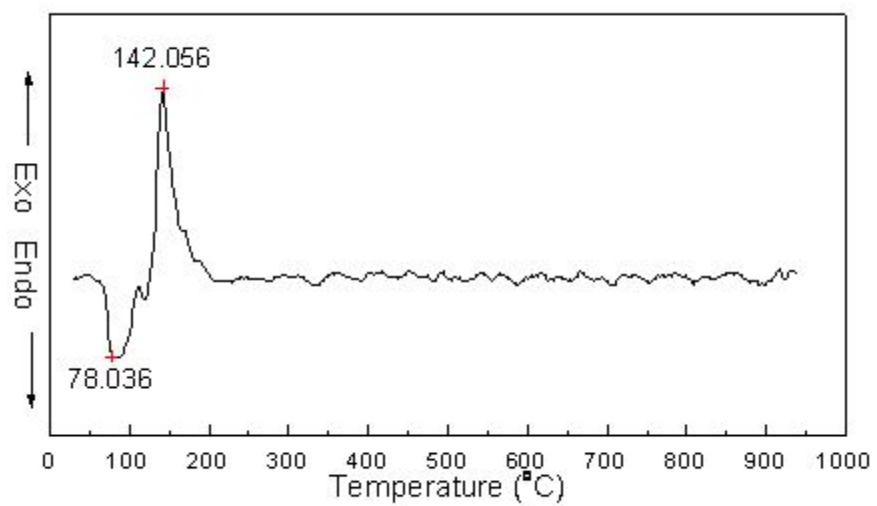


Fig. 2 S.K. Pratihari et. al.

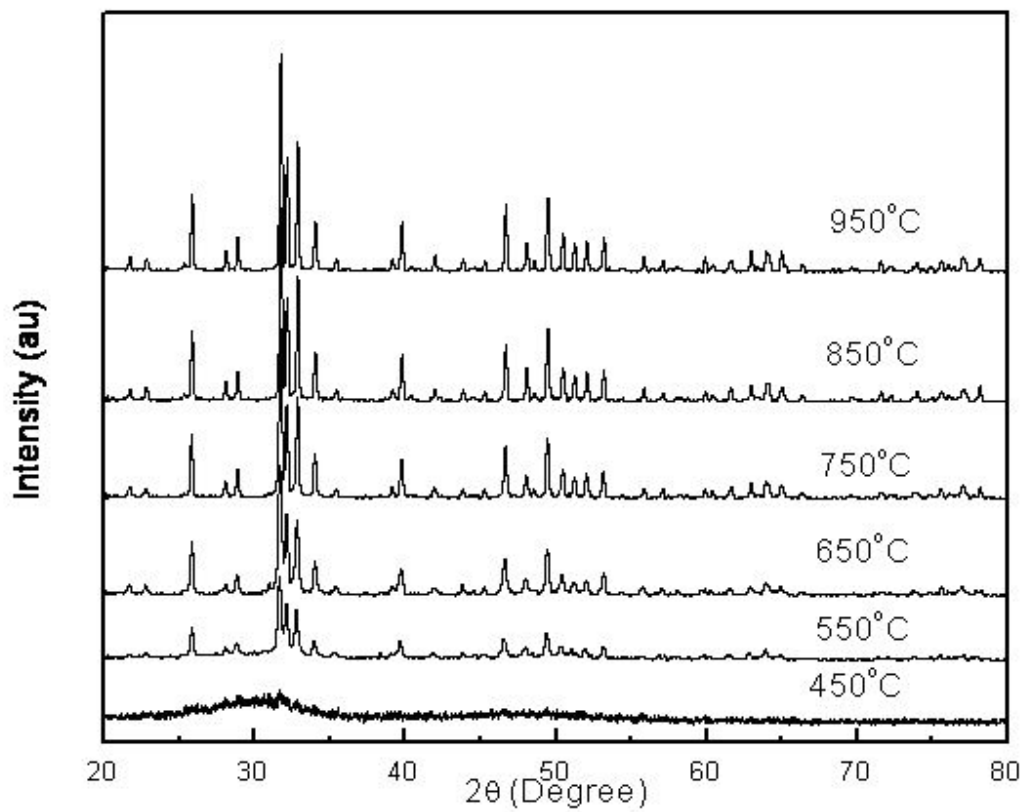


Fig.3 S.K. Pratihari et. al.

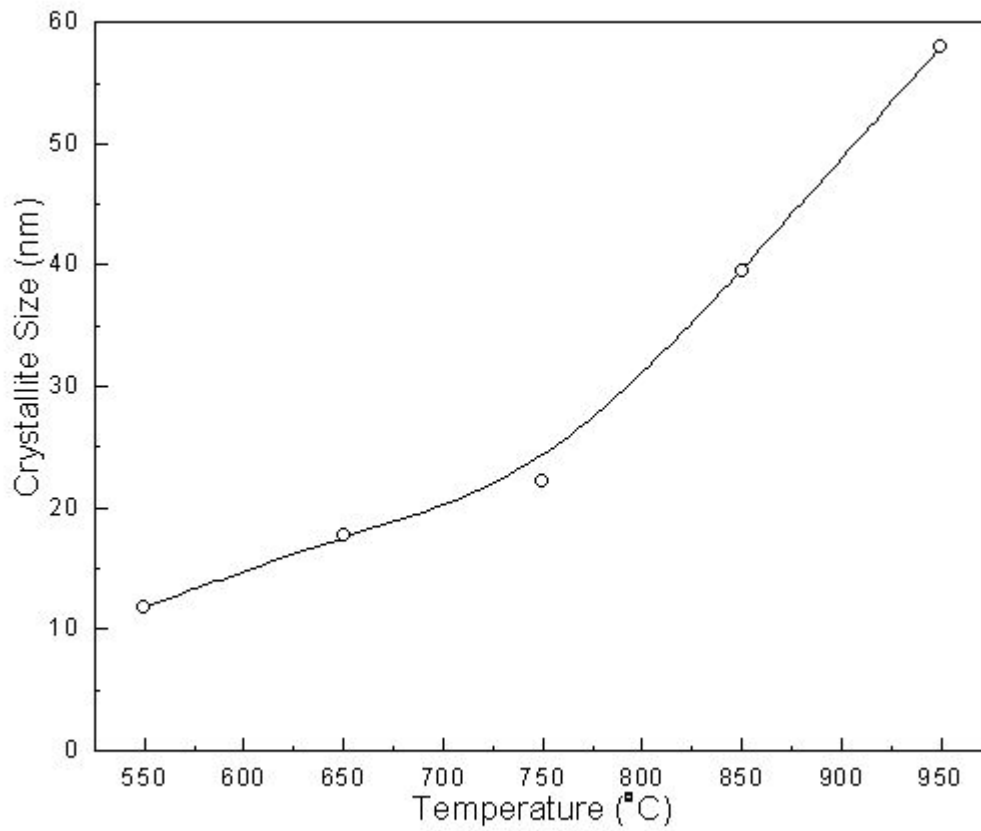


Fig. 4 S.K. Pratihari et. al.

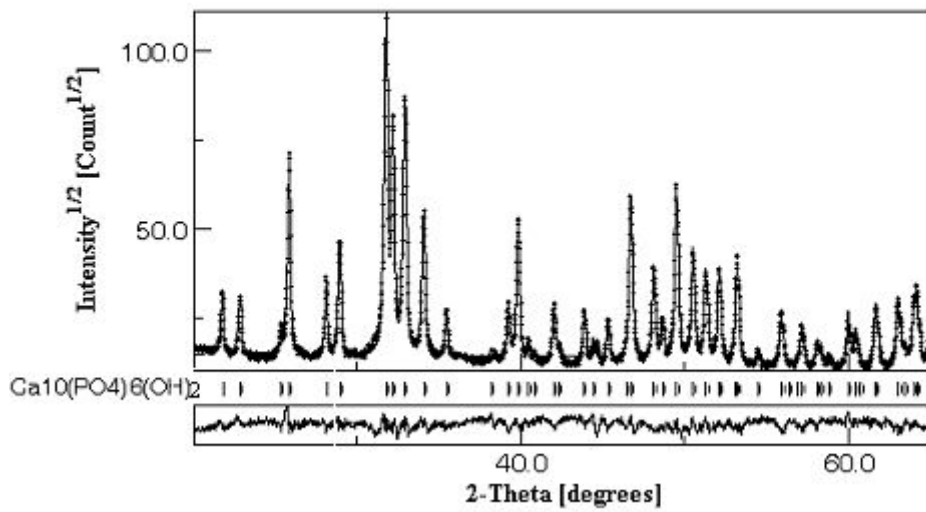


Fig.5 S.K. Pratihari et. al.

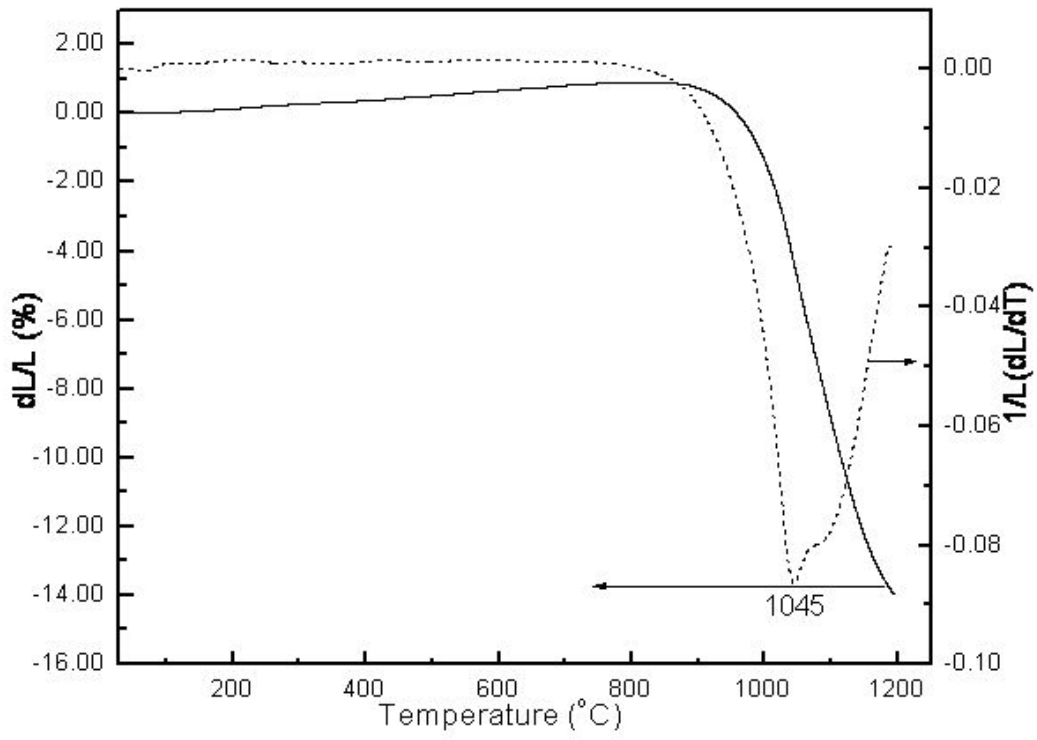


Fig. 6 S.K. Pratihari et. al.

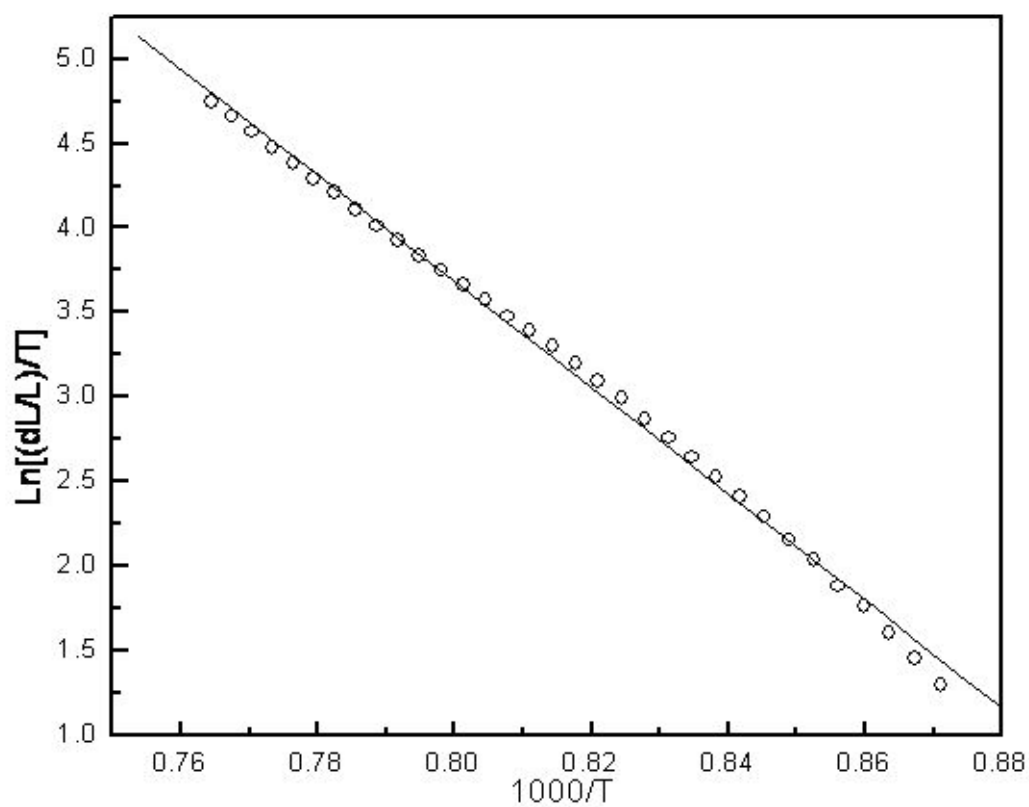


Fig.7 S.K. Pratihari et. al.

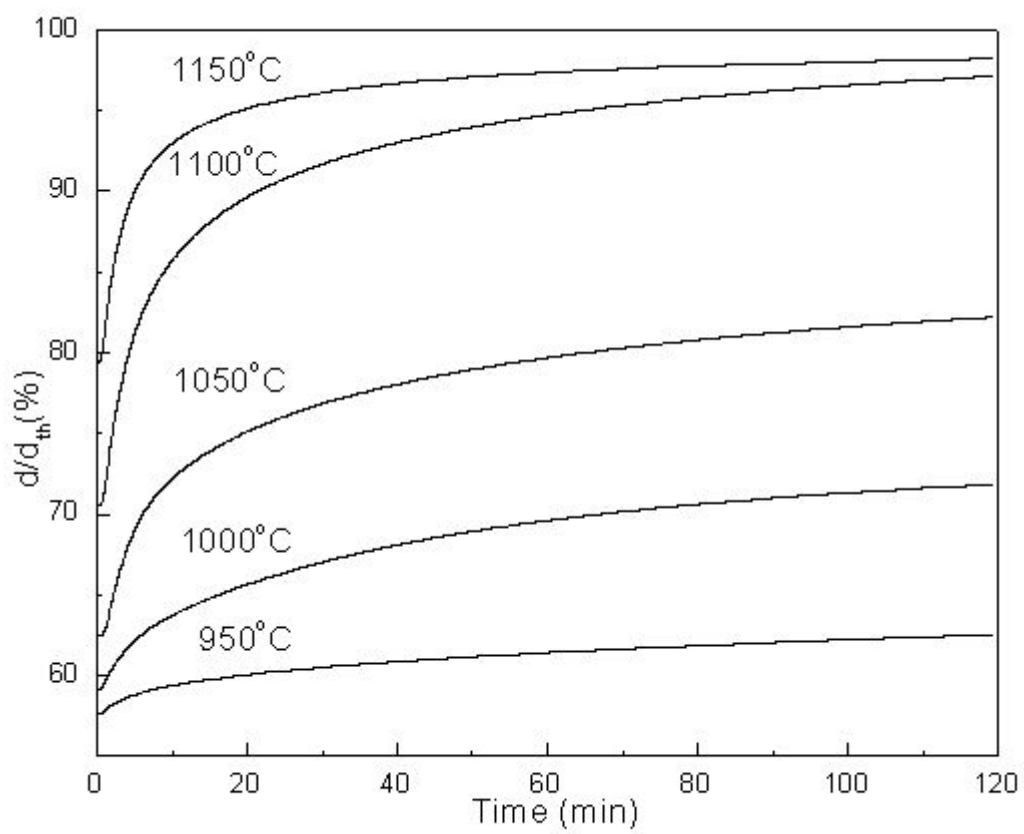


Fig. 8 S.K. Pratihari et. al.

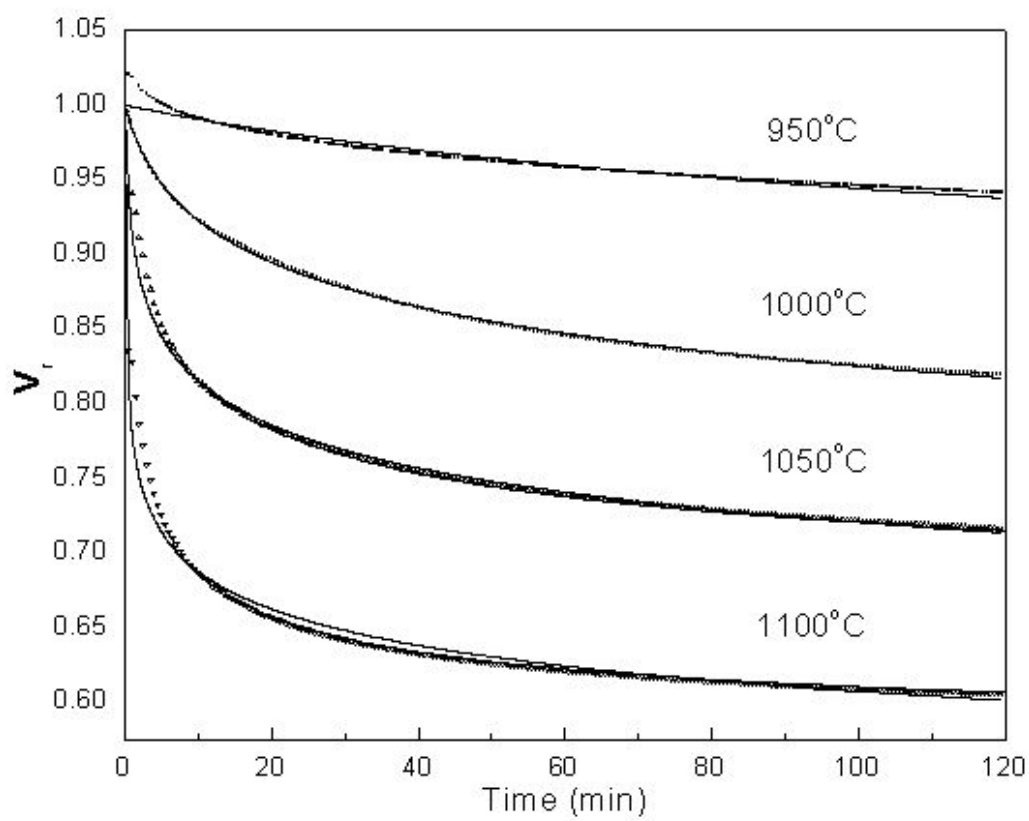


Fig.9 S.K. Pratihari et. al.

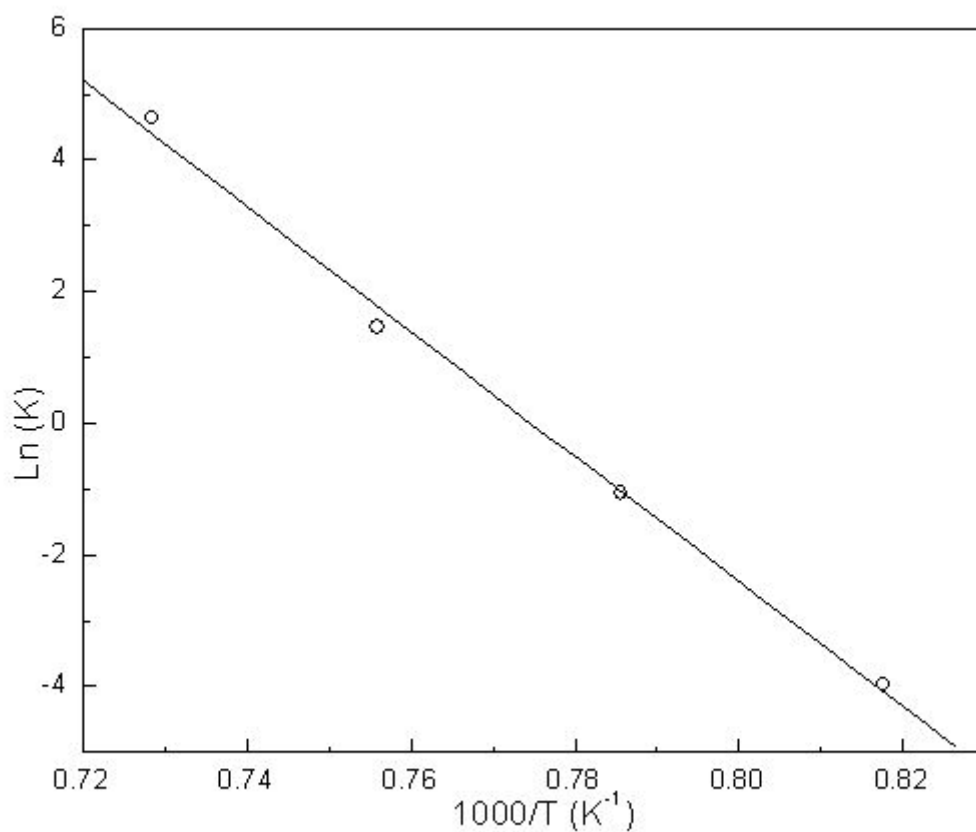


Fig. 10 S.K. Pratihari et.al.

Atoms	X	Y	Z	Occupancy	R _w (%)	R _{wnb} (%)	Lattice parameter (Å ^o)	
							a	c
Ca1	0.6667	0.3333	0.00075	1.000	5.39	4.43	6.8869 (e.s.d = 0.000073)	9.4235 (e.s.d = 0.000081)
Ca2	0.2462	0.2462	0.2500	1.014				
P	0.3998	0.3688	0.2500	0.990				
O1	0.3273	0.4804	0.2500	1.027				
O2	0.5873	0.4681	0.2500	1.021				
O3	0.3342	0.2503	0.0678	1.045				
OH	0.0000	0.0000	0.1814	0.580				
H	0.0000	0.0000	0.1814	0.639				

Table 1 S.K. Pratihari et.al.

